PNAS RESEARCH ARTICLE | DEVELOPMENTAL BIOLOGY

Controllable gap junctions by vitamin B_{12} and light

Duo Cui[a,1], Shuzhang Liu[b,1], Xinyu Huang[a,1], Xiaohan Alex Tang[c], Min Zheng[c], Zonglin He[c], Rui Xu[c], Chenbo Sun[a], Yingjie Xu[a], Renjun Tu[c,d,2], Peng Zou[b,2], Ting Xie[c,2], and Fei Sun[a,e,f,2]

Affiliations are included on p. 11.

Edited by Michael Z. Lin, Stanford University, Stanford, CA; received July 17, 2025; accepted November 14, 2025 by Editorial Board Member Michael Rosbash

Gap junctions mediate rapid signal transduction between contiguous cells, which are indispensable for multicellular organisms to coordinate cellular activities across numerous physiological processes. However, precise control of gap junctions remains elusive. Herein, we present CarGAP, a single-component chemo-optogenetic tool that utilizes the C-terminal adenosylcobalamin ($AdoB_{12}$) binding domain of a photoreceptor protein (i.e., $CarH_C$) to achieve reversible control over both vertebrate and invertebrate gap junctions with spatiotemporal precision. The vertebrate CarGAP (i.e., Cx-CarGAP), created by genetically fusing connexins with $CarH_C$ in mammalian cells, can efficiently block the gap junction channels through $AdoB_{12}$-induced protein oligomerization and subsequently reinstate them via green light–induced protein disassembly. We further introduced the CarGAP system (i.e., Inx-CarGAP) to the *Drosophila* ovary, enabling reversible control over the heterotypic gap junctions formed by innexin2 (Inx2) and innexin4 (Inx4, also known as zero population growth, Zpg), thereby uncovering the roles of gap junctions in stem cell–niche interactions. This study illustrates CarGAP as a generalizable chemo-optogenetic tool for interrogating the functions of gap junctions in various biological contexts.

chemogenetics | gap junction | stem cell niche

Significance

This study introduces CarGAP, a chemo-optogenetic tool that enables precise, reversible control of gap junctions—critical structures for cell-to-cell communication in multicellular organisms. Thanks to its dual response to vitamin B_{12} and light, CarGAP allows researchers to manipulate gap junctions with high spatiotemporal precision in both vertebrate and invertebrate systems. This tool was successfully applied to study gap junction roles in stem cell–niche interactions in *Drosophila*, revealing insights into cellular coordination. CarGAP's versatility makes it a powerful tool for exploring gap junction functions across diverse biological processes, advancing our understanding of cellular communication and its impact on development, physiology, and disease.

Gap junctions are ubiquitous intercellular channels found in virtually all tissues, which intricately connect an array of cell types and facilitate speedy intercellular communications (1). In vertebrates, gap junctions connect adjacent cells via hexameric transmembrane proteins known as connexins, while their counterparts in invertebrate cells use octameric protein complexes known as innexins (2). The evolutionary relationship between connexins and innexins remains enigmatic, given their low sequence homology but high functional similarity (3). The nanometer-sized channels formed by, gap junction channels in adjacent cells allow for their direct exchange of ions (4), second messengers (5–7), microRNAs (8), amino acids (9), and oligopeptides (10), thus impacting a wide range of physiological processes, such as embryonic development (5), immune function (6), cardiac contraction (11), and neuronal synchronization (12, 13). Malfunction of gap junctions has been implicated in various diseases, ranging from cardiovascular disorders (11) to developmental abnormalities (14) and cancer progression (15).

Gap junctions are dynamically regulated under various physiological conditions, ensuring continuous intercellular communication and synchronization between adjacent cells. They may close in response to certain stimuli such as elevated calcium levels (16), abnormal pH (17), or posttranslational modifications (18). In developmental biology, gap junctions are highly expressed in early developmental stages, mediating secondary messenger signaling (19). Traditional genetic methods such as gene knockout/knockdown and loss-of-function mutations, though commonly used, permanently and indiscriminately abolish all functions of gap junction proteins. This fails to differentiate those channel-dependent roles from channel-independent ones and often results in severe consequences such as embryonic lethality (20, 21). In neurobiology, there are two main modalities of synaptic transmission: chemical synapses and electrical synapses, the latter being mediated by gap junctional channels (GJCs) (22). Molecular tools have been disproportionately developed for controlling chemical synapses, but not for GJC-mediated electrical synapses (23–25).

Commonly used small-molecule inhibitors, such as weak organic acids and strong reducing reagents, only partially impair GJC conductance through intracellular acidification and disulfide bond cleavage, respectively. However, these inhibitors often exert adverse nonspecific effects on organisms, limiting their broader applications (26, 27). Peptide-based blockers have been designed to target the loop region of gap junction proteins, offering enhanced specificity and biocompatibility, but they suffer from poor

Author contributions: D.C., S.L., X.H., M.Z., R.T., P.Z., T.X., and F.S. designed research; D.C., S.L., X.H., X.A.T., Z.H., R.X., and R.T. performed research; D.C., S.L., X.H., C.S., Y.X., R.T., P.Z., T.X., and F.S. contributed new reagents/analytic tools; D.C., S.L., X.H., X.A.T., R.T., P.Z., T.X., and F.S. analyzed data; and D.C., S.L., X.H., R.T., P.Z., T.X., and F.S. wrote the paper.

The authors declare no competing interest.

This article is a PNAS Direct Submission. M.Z.L. is a guest editor invited by the Editorial Board.

[1]D.C., S.L., and X.H. contributed equally to this work.

[2]To whom correspondence may be addressed. Email: turenjun@seu.edu.cn, zoupeng@pku.edu.cn, tgx@ust.hk, or kefsun@ust.hk.

This article contains supporting information online at https://www.pnas.org/lookup/suppl/doi:10.1073/pnas.2518037122/-/DCSupplemental.

Published December 23, 2025.

pharmacokinetics due to rapid degradation in vivo (28). Chromophore-assisted light inactivation (CALI) technology has been used to inactivate gap junctions via reactive oxygen species photochemically generated by either genetically encoded EGFP (light intensity: 1.3 MW/cm^2) (29) or a synthetic membrane-permeable, red biarsenical dye bound to tetra-cysteine motifs (light intensity: 17 W/cm^2) (30). Both CALI methods require relatively high light intensities (30, 31). While photocleavable PhoCl has been successfully employed for selective activation of pannexin hemichannels in a pioneering study (32), the development of precise and more gentle methods to control canonical connexin- or innexin-based GJCs—the critical mediators of direct cell-to-cell communication in multicellular organisms—remains an outstanding challenge.

The past several years have witnessed the rapid expansion of optogenetic tools for controlling diverse cellular processes with spatiotemporal precision (33–35). Among them, the vitamin B_{12}–dependent photoreceptor CarH has gained significant traction in both material science and synthetic biology (36–39), due to its unique capacity for dual chemo-optogenetic control, responding to both a small molecule (adenosylcobalamin or $AdoB_{12}$) and light. Identified as a bacterial transcriptional regulator of carotenoid biosynthesis (40, 41), *Thermus thermophilus* CarH consists of an N-terminal DNA-binding domain and a C-terminal $AdoB_{12}$-binding domain ($CarH_C$). In its apo state, $CarH_C$ is monomeric but undergoes tetramerization upon $AdoB_{12}$ binding in the dark. Subsequent green-light illumination triggers the disassembly of tetramers into monomers, accompanied by the cleavage of C-Co, adenosyl release, and formation of bis-His-ligated B_{12} (42). Due to the high photosensitivity of $AdoB_{12}$, even low-intensity green light (μW/cm^2 range) efficiently drives the protein disassembly, pointing to the potential of $CarH_C$ as a gentle and precise tool for optogenetics (38, 43). In this study, by leveraging $CarH_C$, we developed CarGAP, a single-component chemo-optogenetic tool for precise and reversible control of both vertebrate (connexin-based) and invertebrate (innexin-based) GJCs. Using a connexin-based CarGAP, we demonstrated $AdoB_{12}$- and light-dependent regulation of intercellular mass transfer (e.g., fluorescent dyes and 2',3'-cGAMP) and electrical coupling in mammalian cells. Furthermore, innexin-based CarGAPs enabled in vivo investigation of cAMP transport and signaling through heterotypic GJCs in the *Drosophila* germarium, revealing molecular-level insights into stem cell–niche interactions. Given the prevalence and diversity of GJCs, CarGAP offers a powerful approach to dissect their functions in various biological contexts.

Results

Design and Functional Validation of CarGAP in Mammalian Cells. To demonstrate the feasibility of creating chemo-optogenetically controllable gap junctions in living cells, we selected well-characterized connexin 43 (Cx43) (44, 45), the most abundant connexin isoform in vertebrates. As previous studies have shown that placing fluorescent proteins at the C-terminus of Cx43 does not compromise its channel-dependent functionality (46, 47), we created CarGAP by genetically fusing $CarH_C$ at the C-terminus of human Cx43 (GJA1) as well. We conjectured that the possible formation of a dimer-dimers type of tetramer and a dimer upon six $CarH_C$ monomers binding to $AdoB_{12}$ could block the gap junction channel from the intracellular side, thus halting cell-to-cell material exchanges and communications, which could be reversed by $CarH_C$ disassembly induced by green light irradiation, a process that is accompanied with the C-Co cleavage of $AdoB_{12}$ and the bis-His-Co ligation (Fig. 1 *A* and *B* and *SI Appendix*, Fig. S1). Neuro-2a (N2A) cells, a fast-growing mouse neuroblastoma cell line, reportedly show no detectable connexin-based GJCs and therefore can serve as an ideal cellular system for studying recombinant GJCs (48, 49). Most human connexins, including Cx43, have been functionally expressed in N2A cells (50, 51). The N2A cells were genetically engineered to stably express CarGAP via the pLVX-Puro lentiviral expression vector (Fig. 1*C*). To assess the channel function of CarGAP, we performed a dye transfer assay between cocultured CarGAP N2A cells. Donor cells were labeled with two fluorescent dyes, a red- (DiD) or orange-fluorescent (DiI) lipophilic tracer for plasma membranes and green-fluorescent calcein AM for cytoplasmic staining, and then mixed and cocultured with unlabeled CarGAP N2A recipient cells at a ~1:40 donor-to-recipient ratio, following an established protocol (52, 53). The membrane-bound nontransferable DiD served to differentiate the donor cells from the recipient cells, while the hydrophobic calcein AM could be hydrolyzed into hydrophilic calcein molecule upon entering the cytoplasm, of which the transferability from the donor cells to the cocultured recipient cells is highly indicative of the function of GJCs (Fig. 1*D*).

To determine the speed of GJC formation and assess the feasibility of using $AdoB_{12}$ to block gap junctions in cocultured cells, we initially conducted time-course measurements of intercellular dye transfer in N2A cells transiently transfected with CarGAP using Lipofectamine 3000. Flow cytometry analysis of cocultured CarGAP N2A cells revealed little calcein transfer at 3 h postmixing, suggesting insufficient time for reforming GJCs (*SI Appendix*, Fig. S2). By contrast, intercellular calcein diffusion became apparent after 5 h of coculturing, with CarGAP N2A cells adjacent to prelabeled cells displaying clear green fluorescence (Fig. 1*E* and *SI Appendix*, Fig. S2), which thus established 5 h as the optimal timepoint for subsequent functional validation of CarGAP. Wild-type N2A cells showed no dye transfer even after 5 h, consistent with their inherent gap junction deficiency. Moreover, $AdoB_{12}$ potently inhibited CarGAP-mediated coupling throughout the 10-h time course, demonstrating sustained efficacy (*SI Appendix*, Fig. S2). We therefore adopted this method for all further detailed experiments.

To quantitatively evaluate CarGAP-mediated calcein transfer under various conditions, we performed flow cytometry analyses using a stably transfected CarGAP N2A cell line (by lentivirus) cocultured at a donor-to-recipient ratio of ~1:20. The use of stable transfectants, instead of the transient ones, ensured consistent CarGAP expression and minimized experimental variability across replicates. In the absence of $AdoB_{12}$, calcein transfer was observed in 36.0% of CarGAP N2A cells after 5 h of coculturing, increasing to 48.9% by 10 h (Q3 population, green fluorescence only; Fig. 1*E*). $AdoB_{12}$—actively uptaken by cells through receptor-mediated endocytosis (54, 55)—inhibited calcein transfer in CarGAP N2A cells in a dose-dependent manner, with 50 μM $AdoB_{12}$ causing considerable suppression and 500 μM achieving almost complete blockage within 5 h, which rivaled the putative gap-junction inhibitor carbenoxolone (CBX)(56) (*SI Appendix*, Fig. S3). $AdoB_{12}$ (500 μM) further reduced calcein-positive CarGAP N2A cells to just 9.2% (Q3 population) after 10 h of coculturing. This inhibition reached near-baseline levels observed in gap junction-deficient wild-type N2A cells (6.7%) (Fig. 1*E*). The $AdoB_{12}$-induced inhibition persisted under dark conditions, remaining effective even after phosphate-buffered saline (PBS) washing and an additional 5 h of coculturing. Nevertheless, brief green light exposure (5 min) completely reversed this blockage, restoring transfer efficiency to 31.8% of recipient cells in Q3. In contrast, MeB_{12}, a vitamin B_{12} variant that binds to $CarH_C$ without inducing oligomerization (57), showed minimal effect on calcein transfer, with 35.9% (5 h) and 44.2% (10 h) of recipient cells remaining in Q3, suggesting that $CarH_C$ oligomerization is required for channel inhibition.

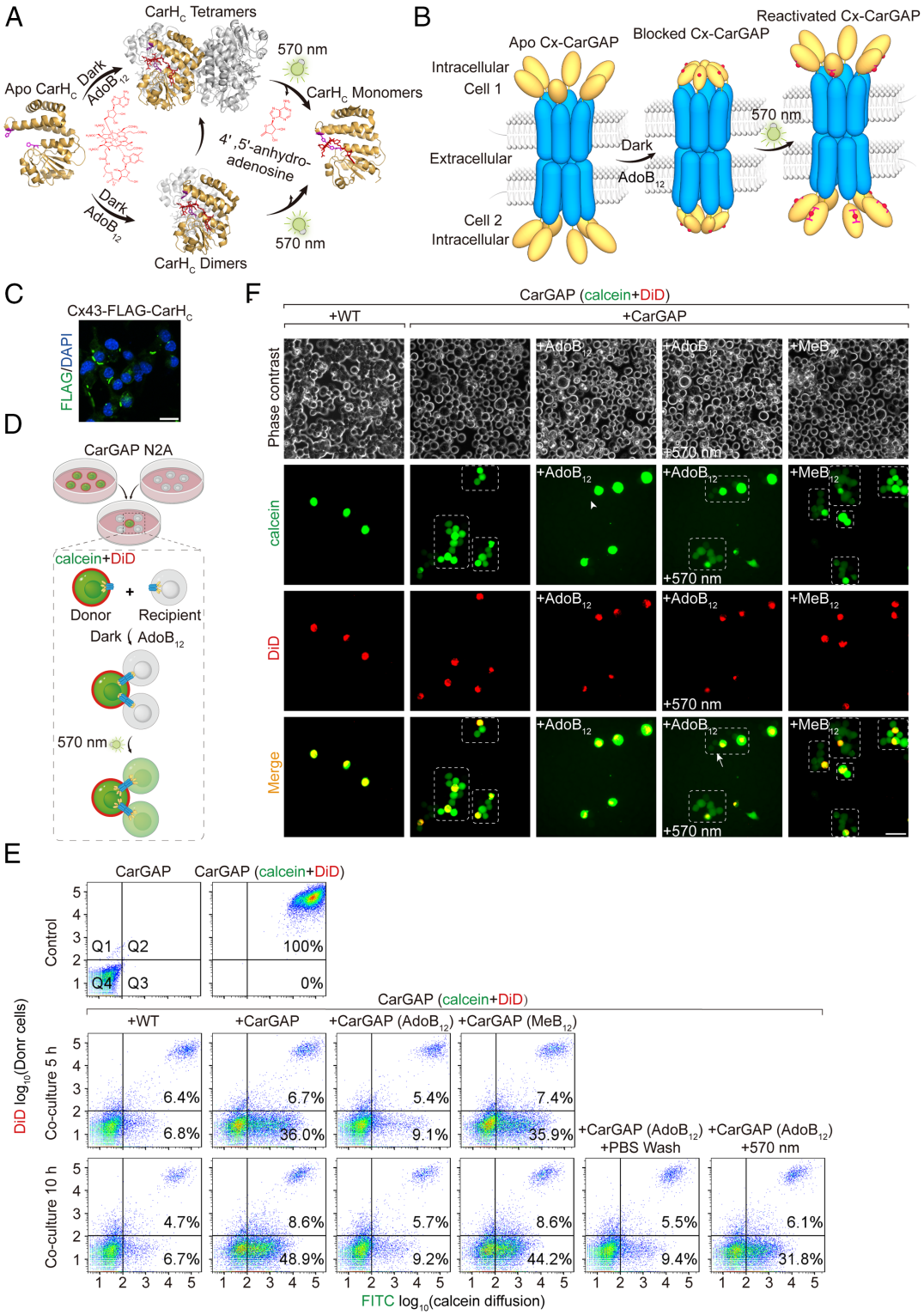

Fig. 1. Chemo-optogenetic control of intercellular dye transfer via connexin–CarGAP. (*A*) Photochemistry of CarH$_C$. In the dark, CarH$_C$ monomers bind AdoB$_{12}$ to form oligomers (PDB: 5C8A). Green light (570 nm) triggers disassembly into monomers (PDB: 5C8F) via AdoB$_{12}$ photolysis, releasing 4′,5′-anhydroadenosine. (*B*) Design of Cx-CarGAP as a molecular valve for gap junctions. AdoB$_{12}$ induces CarH$_C$ oligomerization to block intercellular channels in the dark; 570 nm illumination restores channel function. (*C*) Immunofluorescence image of a stable N2A cell line expressing Cx43-FLAG-CarH$_C$. (Scale bar, 20 μm.) Construct details in *SI Appendix*, Table S1. (*D*) Coculture assay schematic. Donor cells were dual-labeled with DiD (red; membrane-bound and gap junction–impermeant) and membrane-permeant calcein-AM (green; hydrolyzed intracellularly to calcein that is gap junction–permeant but membrane-impermeant, 623 Da). These were mixed with unlabeled recipients at ~1:40 ratio (~1:20 for flow cytometry) and plated at ~50,000 cells/cm^2. AdoB$_{12}$ was added in the dark to inhibit calcein transfer; 570-nm light (10 mW/cm^2, 5 min) reactivated transfer. (*E*) Flow cytometry analysis of dye transfer. Cells cocultured at ~1:20 ratio for 5 to 10 h were analyzed by FACS: dual-positive donors (DiD$^+$/calcein$^+$) in Q2; calcein$^+$ recipients in Q3. Corresponding FITC histograms in *SI Appendix*, Fig. S4. (*F*) Fluorescence images showing calcein transfer between N2A cells under various conditions: CarGAP to Cx43-deficient WT, CarGAP to CarGAP, +AdoB$_{12}$ (500 μM, dark), +AdoB$_{12}$ (500 μM) → 570 nm light, and +MeB$_{12}$ (500 μM, dark). Donors: DiD$^+$/calcein$^+$ (red/green); recipients: calcein$^+$ (green). The "+AdoB$_{12}$ + 570 nm" panel was acquired in situ from the same fields of view within the same samples as the "+AdoB$_{12}$" panel. Dashed boxes highlight regions with intercellular calcein transfer. (Scale bar, 50 μm.) Data are representative of at least three independent experiments.

Complementing our flow cytometry data, fluorescence microscopy confirmed complete suppression of calcein transfer in $AdoB_{12}$-treated CarGAP N2A cells under dark conditions, demonstrating that $AdoB_{12}$-induced $CarH_C$ oligomerization effectively blocks channel function. This inhibition can be readily reversed, with 5-minute green light exposure (10 mW/cm^2) fully restoring intercellular calcein diffusion (Fig. 1*F*). Once again MeB_{12}—which cannot induce $CarH_C$ oligomerization—failed to inhibit dye transfer (Fig. 1*F*), further establishing oligomerization as the essential mechanism for channel blockage.

Collectively, these results establish connexin-based CarGAP as a robust chemo-optogenetic platform for reversible regulation of GJC-mediated molecular transfer in mammalian cells.

Chemo-Optogenetically Controlled Transport of 2′3′-cGAMP Across Mammalian Cells. The second messenger, 2′3′-cyclic GMP-AMP (2′3′-cGAMP), plays a pivotal role in innate immunity and viral defense (58). In a canonical process, 2′3′-cGAMP, synthesized by cyclic GMP-AMP synthase (cGAS) in response to cytosolic double-stranded DNA, activates the stimulator of interferon genes (STING) signaling pathway within the producing cells, which further triggers a cascade of antiviral responses in a type I interferon-dependent manner (58). Alternatively, in a process known as bystander immunity (6), 2′3′-cGAMP transfers from producing cells to adjacent cells through connexin gap junctions, thus promoting STING signaling and antiviral immunity in the abutted cells independently of type I IFN signaling. Upon activation by cGAMP, STING undergoes oligomerization and assembles into a supramolecular complex. This triggers its translocation from the endoplasmic reticulum (ER) to the perinuclear Golgi apparatus, a process readily detectable by fluorescence microscopy (59) (Fig. 2*A*). Native N2A cells, while lacking intrinsic Cx43 and STING, possess endogenous cGAS capable of sensing and responding to cytosolic double-stranded DNA (dsDNA), such as plasmids. This characteristic hampers their utility as a model cell line for the transient transfection of *STING*, as it can lead to autoactivation following transfection (*SI Appendix*, Fig. S5). In contrast, native HEK293T cells do not express either cGAS or STING (60) but possess abundant endogenous gap junctions, including Cx43. Moreover, coculturing the two cell lines indeed formed functional gap junctions, as evidenced by the pronounced calcein transfer from CarGAP N2A cells to neighboring HEK293T cells (Fig. 2*B*). The complementarity between N2A cells and HEK293T cells renders them ideal donors and recipients, respectively, to examine the possibility of controlling intercellular transport of 2′3′-cGAMP. To accomplish this, we boosted the synthesis of cGAMP in both WT and CarGAP N2A cells by transiently overexpressing cGAS, along with HT-DNA activation, followed by mixing and coculturing with the recipient HEK293T cells transiently transfected with *STING-egfp* at a ratio of ~1:40 (Fig. 2*C*).

Contrary to WT N2A cells, which failed to elicit any bystander STING-EGFP translocation from ER to Golgi in adjacent HEK293T cells owing to the absence of functional gap junctions and intercellular cGAMP transport, CarGAP N2A cells were surrounded by HEK293T cells that exhibited clear STING-EGFP translocation, indicative of functional gap junction channels that mediated the transport of cGAMP from the producing CarGAP N2A cells to the nearby HEK293T cells. The intercellular transport of cGAMP was inhibited by $AdoB_{12}$, as evidenced by few HEK293T cells with STING-EGFP translocation in the cocultures in the presence of $AdoB_{12}$ in the dark, strongly suggesting the blockage of CarGAP channels. Once again, $CarH_C$ oligomerization proved to be essential for the blockage of CarGAP channels and thus the transport of cGAMP, as MeB_{12}, which binds to $CarH_C$ but induces no oligomerization, exerted almost no effect on STING-EGFP in HEK293T, of which translocation remained.

Notably, STING activation in HEK293T cells was heterogeneous, with some cells adjacent to N2A donors remaining unactivated while some seemingly distant responded. This heterogeneity likely arises from the discontinuous gap junction network formed by the three-dimensionally clustered N2A cells, which restricts cGAMP delivery only to HEK293T cells that form direct lateral membrane contacts. Cells appearing adjacent in two-dimensional projection may actually be vertically separated or connected only apically, thus precluding functional coupling. Meanwhile, distant activation can be explained by cGAMP diffusion through endogenous connexin channels within the HEK293T monolayer, relaying the signal beyond the immediate donor interface. Additionally, the fixed imaging field may capture cGAMP transfer originating from N2A donors located just outside the frame, further contributing to the observed heterogeneity.

The blockage of cGAMP transport from CarGAP N2A to HEK293T cells by $AdoB_{12}$ was eliminated following a 5-minute green light irradiation, leading to considerable STING-EGFP translocation in the HEK293T cells (Fig. 2 *D* and *E* and *SI Appendix*, Fig. S6). By contrast, the green light irradiation alone did not cause any detectable perturbation to cell states, dye transport in WT N2A/CarGAP N2A (without $AdoB_{12}$) cocultures, and cGAMP transport in WT N2A/HEK293T cocultures or CarGAP N2A/HEK293T (without $AdoB_{12}$) cocultures, confirming that the observed effects of green light are specifically dependent on the combination of $AdoB_{12}$ and CarGAP (*SI Appendix*, Fig. S7). Taken together, these results not only corroborated the critical roles of gap junctions in cGAS-STING signaling and bystander immunity but also highlighted the feasibility of using this chemo-optogenetic approach to control the intercellular transport of crucial second messengers.

Chemo-Optogenetic Control and Far-Red Fluorescent Recording of Electrical Coupling Among Adjacent Cells. Gap junctions enable the instantaneous and reciprocal spread of current among adjacent cells (22). The traditional patch-clamp technique has often been used to study electrophysiology in individual cells. However, applying this method to multiple cells connected through gap junctions remains challenging. It is therefore highly desirable to have a technique that not only enables precise control over the electrical coupling and dynamics within cell clusters but also facilitates straightforward recording of these events. Regarding the control of electrical coupling, CarGAP has provided a chemo-optogenetic way to modulate gap junction channels and therefore holds great promise for controlling electrical coupling across multiple cells. In terms of recording electrical dynamics, a series of hybrid fluorescent membrane voltage indicators have recently been created via the site-specific modification of rhodopsin proteins with synthetic small-molecule fluorophores. These indicators have enabled the optical mapping of gap junction-mediated electrical couplings across a monolayer of HEK293T cells (61). We envisioned that combining the chemo-optogenetic tool CarGAP with the hybrid voltage indicators could lead to a methodology capable of chemo-optical control while also optically recording the electrical dynamics in an interconnected multicellular system. To avoid interfering with CarGAP, which is sensitive to green light, we selected a far-red hybrid voltage indicator, NAVI-Cy5, that responds to membrane voltage changes via the electrochromic Förster resonance energy transfer (eFRET) mechanism (62) (Fig. 3*A*).

To examine the integrated use of CarGAP and NAVI-Cy5 in electrophysiology, we employed HeLa cells, which are substantially larger than N2A cells and thus more amenable to patch clamping. WT HeLa cells possess basal-level gap junctions composed of

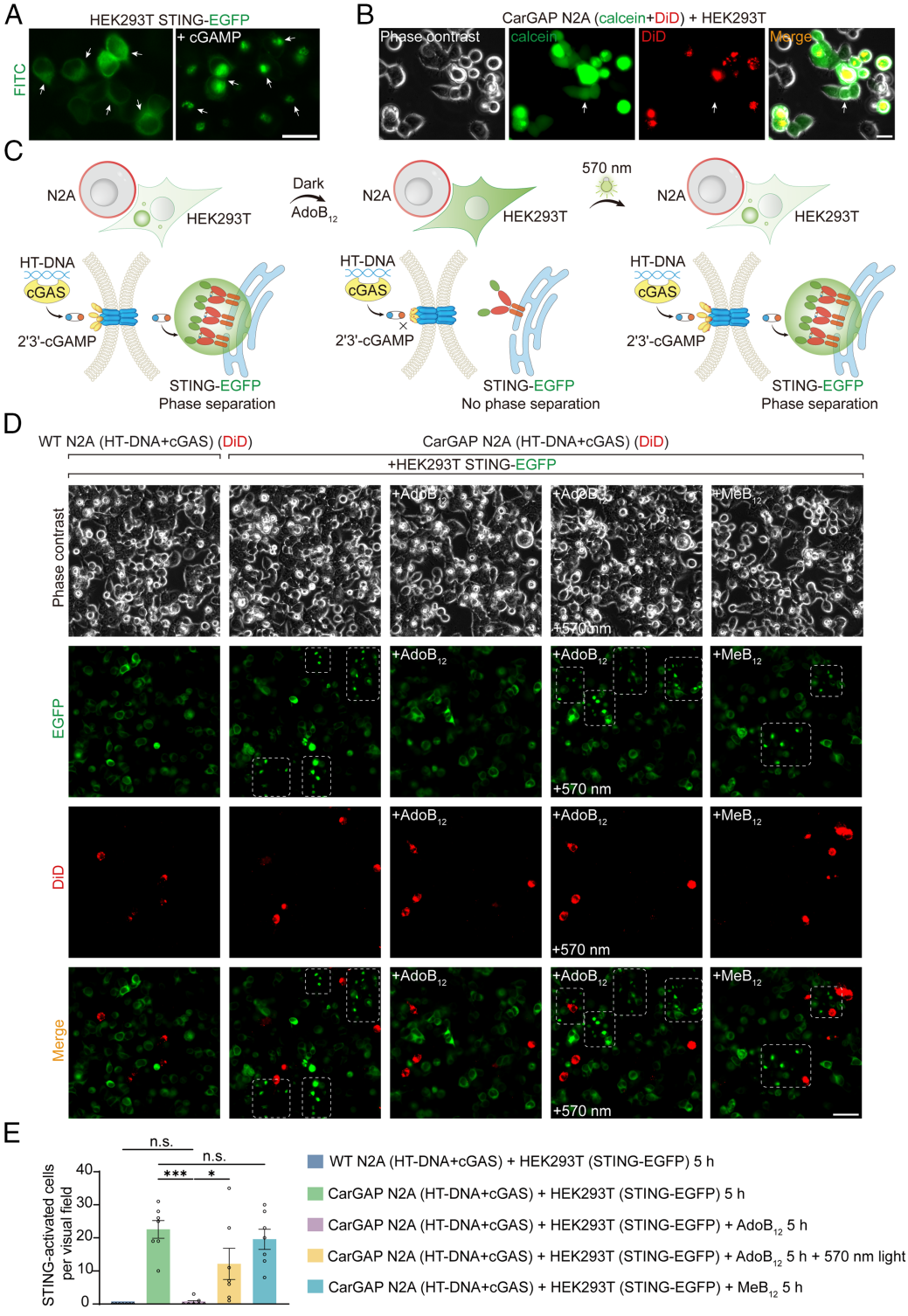

Fig. 2. Chemo-optogenetic control of intercellular 2′3′-cGAMP transfer via connexin–CarGAP. (*A*) STING-EGFP oligomerization and translocation in HEK293T cells following exogenous cGAMP delivery. (Scale bar, 20 μm.) (*B*) CarGAP-mediated calcein transfer from CarGAP N2A cells to adjacent HEK293T cells. (Scale bar, 20 μm.) (*C*) Schematic representation of CarGAP-controlled cGAMP transport. $AdoB_{12}$-induced CarGAP closure blocks cGAMP transfer from N2A to HEK293T cells; 570 nm illumination restores transport. (*D*) Coculture assay showing ER-to-Golgi translocation of STING-EGFP in HEK293T cells induced by cGAMP transfer through CarGAP. cGAS (activated by HT-DNA) and STING-EGFP were transiently expressed in N2A and HEK293T cells, respectively, using Lipofectamine 3000. DiD-labeled N2A cells were cocultured with STING-EGFP HEK293T cells for 5 h under four conditions: no B_{12}; +$AdoB_{12}$ (500 μM, dark); +$AdoB_{12}$ → 570 nm light (10 mW/cm^2, 5 min) → 5 h recovery; +MeB_{12} (500 μM, dark). The "+$AdoB_{12}$+570 nm" panel was acquired in situ from the same fields of view within the same samples as the "+$AdoB_{12}$" panel. Dashed boxes highlight regions with cGAMP-dependent STING-EGFP translocation. (Scale bar, 50 μm.) (*E*) Quantification of STING-activated HEK293T cells adjacent to N2A donors. Data are presented as mean ± SEM (n = 7 fields of view); two-sided *t* test: **P* < 0.05, ****P* < 0.001, n.s. (not significant).

connexin45 (Cx45) (63). As a result, the WT HeLa cells surrounding the patched exhibited an average voltage response of 35.9 ± 4.8% relative to the patched cell, suggesting a weak but non-negligible electrical coupling (Fig. 3 *B* and *C*). Therefore, we created a *Cx45*-knockout cell line, CarGAP HeLa, that stably produces CarGAP. The engineered cells adjacent to the patched

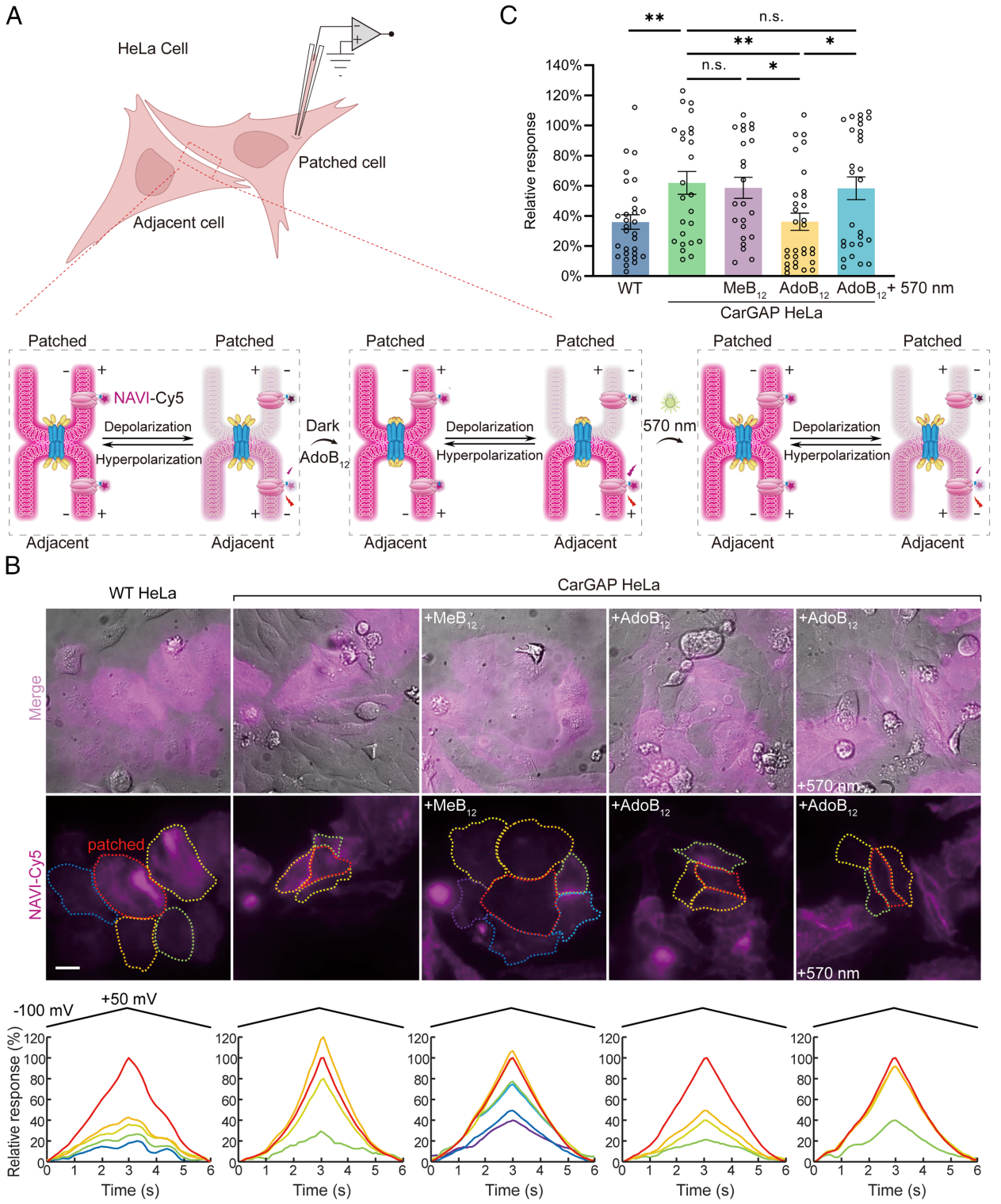

Fig. 3. Chemo-optogenetic control of electrical coupling via CarGAP. (*A*) Schematic of CarGAP-controlled electrical coupling in HeLa cells visualized with the voltage sensor NAVI-Cy5. NAVI-Cy5 detects changes in membrane potential through an electrochromic FRET mechanism; membrane depolarization results in decreased Cy5 fluorescence emission, while hyperpolarization leads to increased emission. (*B*) Representative images of switchable electrical coupling. "WT HeLa" indicates wild-type HeLa cells; "CarGAP HeLa" denotes Cx43-knockout cells stably expressing Cx43-CarH$_C$. Cells were treated with 500 μM MeB$_{12}$, or AdoB$_{12}$ for 6 h; "+AdoB$_{12}$ + 570 nm" indicates AdoB$_{12}$-treated cells subsequently illuminated for 5 min (550 to 590 nm filter, ~3 W/cm^2). Patched cells (red dashed outlines) were stimulated with a triangle waveform (−100 to +50 mV, 10 Hz). Normalized Cy5 fluorescence intensities (637 nm excitation) are shown from 0 (−100 mV) to 100% (+50 mV). (Scale bar, 20 μm.) (*C*) Quantification of electrical coupling between patched cells and adjacent cells. Data are presented as mean ± SEM (n = 30, 25, 23, 31, and 28 adjacent cells); two-sided *t* test: **P* < 0.05, ***P* < 0.01, n.s. (not significant).

cells exhibited an average voltage response of 61.9 ± 7.6 %, substantially higher than that of WT HeLa cells. This finding indicated that CarGAP channels enabled stronger electrical coupling than the native Cx45 channels in HeLa cells.

The voltage response of the CarGAP HeLa cells diminished to 36.1 ± 5.7 %, after treatment with 500 μM AdoB$_{12}$ for 6 h, in contrast, the response remained largely unchanged (58.4 ± 7.0 %) when cultured with 500 μM MeB$_{12}$, demonstrating that

$AdoB_{12}$-induced $CarH_C$ oligomerization is essential for blocking CarGAP channels and decoupling the electrical signals among the cells (Fig. 3 *B* and *C*). Upon green light exposure (3 W/cm^2, 5 min), the electrical coupling was restored to the level observed in the absence of $AdoB_{12}$, with a comparable voltage response of 58.3 ± 7.5% (Fig. 3 *B* and *C*). These results showcased the reversible control and facile optical recording of dynamic electrical coupling among interconnected cells enabled by the combination of the chemo-optogenetic tool CarGAP and the far-red hybrid voltage indicator NAVI-Cy5, pointing a unique approach to studying electrophysiology in complex multicellular structures.

Chemo-Optogenetically Controlled Intercellular CAMP Transport in the *Drosophila* germarium. While CarGAP has shown its might in controlling mass transfer and electrical coupling among adjacent mammalian cells in vitro, it remains to be seen whether this tool can also exert a delicate control over cellular signaling in more complex biological systems. Gap junctions in invertebrates such as *Drosophila* mainly consist of innexins, of which two octameric complexes docked together to form a gap junction channel (64). In the *Drosophila* ovary, inner germarial sheath (IGS) cells form the niche for controlling germline stem cell (GSC) self-renewal and differentiation (65); heterotypic gap junctions composed of niche-specific Inx2 and germ cell–specific Inx4 transport cyclic AMP (cAMP) from niche cells to GSCs and their progeny, thereby orchestrating stepwise oocyte differentiation and development (5). We envisioned that the ability to dynamically control the flow of crucial second messengers such as cAMP via gap junctions in vivo will open a synthetic biology approach for biological regulation. To explore this possibility, we constructed two CarGAP systems, i.e., niche-specific Inx2-CarGAP (Fig. 4*A*) and GSC/progeny-specific Inx4-CarGAP (*SI Appendix*, Fig. S9*A*), by genetically fusing $CarH_C$ to the C termini of Inx2 and Inx4, respectively. To functionally replace the native IGS-specific Inx2 with Inx2-CarGAP in the *Drosophila* ovary, we created transgenic flies harboring the RNAi-resistant (RR) gene construct, *UASz-inx2^{RR}-FLAG-carH$_C$* (Fig. 4*B*).

To verify the expression of Inx2-FLAG-$CarH_C$ in IGS cells, we first employed the somatic cell–specific c587-Gal4 driver (*SI Appendix*, Fig. S8*A*) (66). For enhanced experimental flexibility in fly crosses, we subsequently developed a thermal induction system using the *13C06-Gal4* driver, which similarly targets somatic cells, including IGS cells, follicle stem cells (FSCs), and prefollicle cells adjacent to the region 2a/2b border (67). In this system, denoted as *inx2KD+inx2^{RR}-carH$_C$*, the transcription factor Gal4 is driven by the 13C06 (a tissue-specific promoter strongly expressed in IGS cells); Gal80^{ts}, a temperature-sensitive inhibitor of Gal4, is driven by tub (a constitutively active tubulin promoter). At an ambient temperature of 20 °C, Gal4 expression is repressed by Gal80^{ts}. However, at an elevated temperature of 29 °C, Gal80^{ts} repression is lifted, allowing Gal4 to activate the expression of *inx2^{RR}-FLAG-CarH$_C$* through its upstream activating sequence (UAS). Concurrently, *inx2 shRNA* is coexpressed to selectively knock down the native *inx2* gene (Fig. 4*C*). In a similar vein, to incorporate the GSC/progeny-specific Inx4-CarGAP into the *Drosophila* ovaries, we first use the germline specific *nos-Gal4* driver (68) to verify the expression of Inx4-HA-$CarH_C$ in germ cells. Further, we made the transgenic flies to possess the gene constructs, including *UASz-inx4^{RR}-carH$_C$* and *UAS-shRNA*, along with the germline-specific *nos-GeneSwitch-Gal4* driver (mainly expressed in 2a region during germarium development) to achieve the genetic replacement of the endogenous *inx4* to *inx4-carH$_C$* (*SI Appendix*, Figs. S8*B* and S9 *B* and *C*). The GeneSwitch-Gal4, which combines the Gal4/UAS system with a receptor of RU486 (mifepristone) (69), allowed us to activate the expression of *inx4^{RR}-carH$_C$* in response to the administration of RU486, while coexpressing *inx4 shRNA* to silence the native *inx4* gene (*SI Appendix*, Fig. S9*C*).

To assess the influence of CarGAP on relative distributions of cAMP under various conditions, we used a commercial rabbit anti-cAMP monoclonal antibody to fluorescently stain and quantify this second messenger in the ovaries. The relative fluorescence intensities of cystocyte clusters and their surrounding IGS cells would reflect the transferability of cAMP from IGS cells (somatic cells) to the germline (GSCs, cystoblasts [CBs], cystocytes) (Fig. 4*D* and *SI Appendix*, Fig. S9*D*). Detailed methods for quantifying cAMP fluorescence intensity in IGS/germline cells are provided in Fig. 4*E* and *SI Appendix*, Fig. S9*E*. Consistent with the previous finding that gap junctions are essential for the cAMP transport in the ovaries (5), knocking down either *inx2* or *inx4* disrupted the cAMP transport from IGS cells to germ cells, as evidenced by the contrast in fluorescence between these cells (Fig. 4*E* and *SI Appendix*, Fig. S9*E*). Expression of Inx2-CarGAP in the *inx2KD* germarium (i.e., *inx2KD+inx2^{RR}-carH$_C$*) or Inx4-CarGAP in the *inx4KD* germarium (i.e., *inx4KD+inx4^{RR}-carH$_C$*) restored the flow of cAMP from IGS cells to germ cells, confirming the functionality of the Inx-CarGAP channels (Fig. 4 *D–F* and *SI Appendix*, Fig. S9 *D–F*). Given the bidirectional nature of gap junctions, IGS-specific Inx2-CarGAP and Germline-specific Inx4-CarGAP should be functionally indistinguishable and chemo-optogenetic control over the cAMP transport may be accomplished from either side, IGS cells or Germline (Fig. 4*D* and *SI Appendix*, Fig. S9*D*). Consistent with this prediction, orally feeding both transgenic flies (i.e., *inx2KD+inx2^{RR}-carH$_C$* and *inx4KD+inx4^{RR}-carH$_C$*) with $AdoB_{12}$ for two days stemmed the flow of cAMP from IGS cells to germ cells, leading to its accumulation and depletion in IGS cells and germ cells, respectively. By contrast, feeding the flies with MeB_{12} failed to do so, suggesting that $AdoB_{12}$-induced $CarH_C$ oligomerization is essential for the observed inhibition of CarGAP channels in vivo (Fig. 4 *D–F* and *SI Appendix*, Fig. S9 *D-F*). To examine whether light-induced protein disassembly can restore the cAMP transport, we placed these transgenic flies under green light irradiation (570 nm, 80 mW/cm^2) (*SI Appendix*, Fig. S10*B*). It turned out that brief light exposure for merely 5 min was sufficient to increase cAMP in germ cells to a level comparable to that of the control, strongly suggesting the resumed flow of cAMP among the cells (Fig. 4 *D–F* and *SI Appendix*, Fig. S9 *D–F*). These results highlighted CarGAP as a robust chemo-optogenetic tool for reversibly controlling the intercellular transport of the crucial second messenger cAMP in complex biological systems.

Modulating Ovarian Development via CarGAP. Tu and coworkers recently showed that IGS-specific Inx2 proteins form gap junctions with GSC/progeny-specific Inx4 proteins in the *Drosophila* ovary, which further dictate stepwise GSC lineage development, including GSC self-renewal, germline cyst formation, meiotic double-strand DNA break (DSB) formation, and oocyte specification (5). While *inx2* knockdown (i.e., *inx2KD*) led to pronounced phenotypic defects in the ovaries, such as fewer GSCs, more CBs, decreased *H2AvD* expression, and double oocytes in stage 1 egg chambers, the expression of *inx2^{RR}-FLAG-carH$_C$* in the *inx2KD* background (i.e., *inx2KD+inx2^{RR}-carH$_C$*) at 29 °C restored these ovarian phenotypes to a level comparable to the WT control, supporting the normal function of Inx2-CarGAP in vivo (Fig. 5 *A–D*). Interestingly, simply feeding the *inx2KD+inx2^{RR}-carH$_C$* fruit flies with $AdoB_{12}$ powders, but not MeB_{12}, sufficiently caused severe ovarian defects in GSC maintenance, CB differentiation, meiotic DSB formation, and aberrant oocyte determination akin to *inx2KD*, showing that $AdoB_{12}$-induced $CarH_C$ oligomerization can efficiently block the gap junction channels in vivo (Fig. 5 *A-D*). Reminiscent of

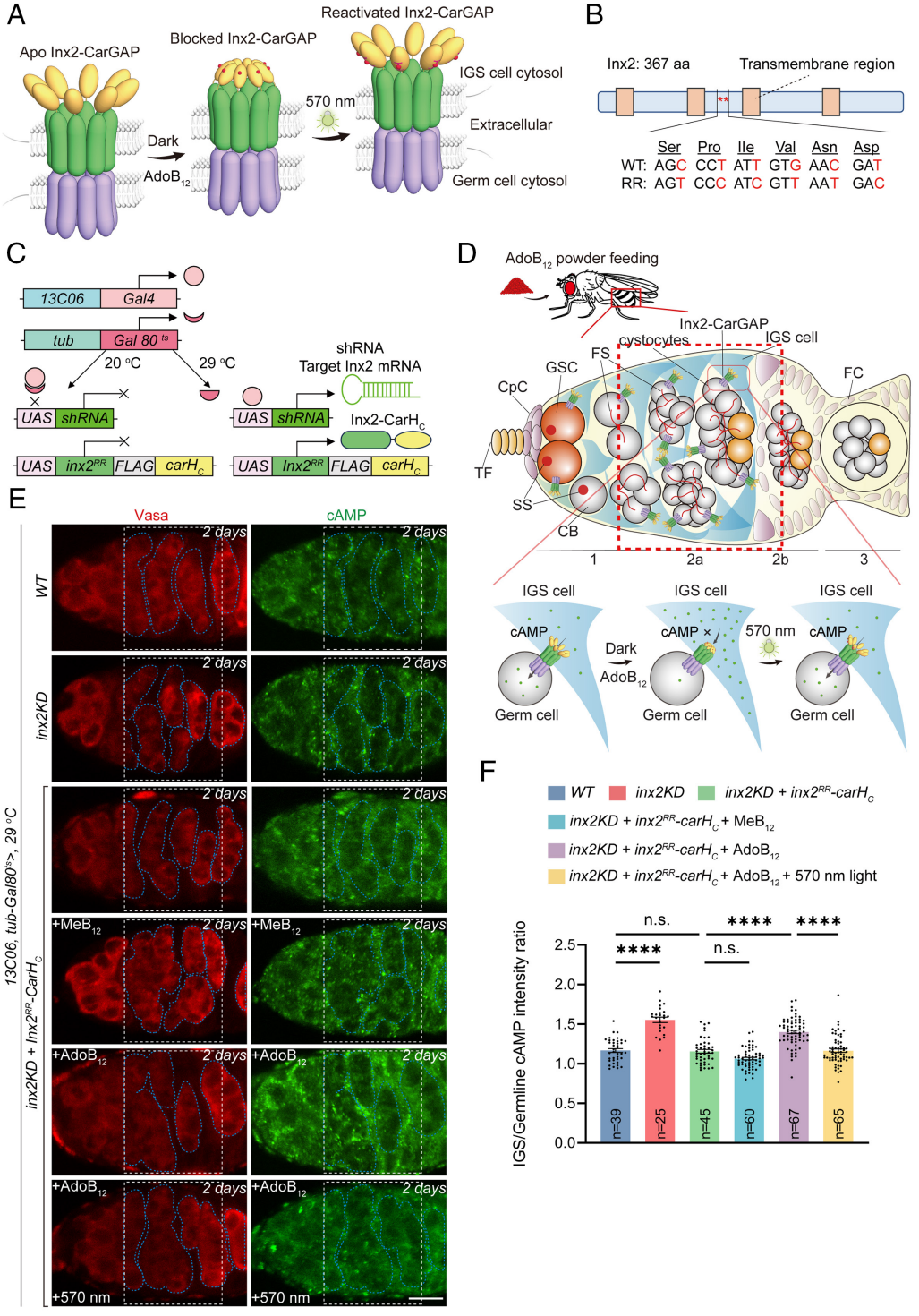

Fig. 4. Chemo-optogenetic control of intercellular cAMP transport in *Drosophila* germaria via Inx2–CarGAP. (*A*) Schematic of Inx2-CarGAP. $AdoB_{12}$ binding induces $CarH_C$ oligomerization, blocking the heterotypic gap junction channel within IGS cells; 570 nm illumination reactivates channel function. (*B*) Domain architecture of Inx2 and design of the RNAi-resistant *inx2* replacement. Synonymous codon substitutions were introduced in the shRNA-targeted region (BDSC #80409). (*C*) Genetic strategy for temperature-dependent Inx2-CarGAP expression using *13C06-Gal4* and *tub-Gal80^{ts}*. At 20 °C, Gal80^{ts} inhibits Gal4; at 29 °C, Gal80^{ts} inactivation permits UAS-driven expression of *inx2* shRNA and RNAi-resistant *inx2-carH$_C$*. (*D*) Model of CarGAP-controlled cAMP efflux from IGS cells within a *Drosophila* germarium. Dietary $AdoB_{12}$ blocks cAMP transport in the dark; 570 nm illumination restores the transport. (*E*) Confocal images of cAMP distribution (anti-cAMP, green) and germline (anti-Vasa, red). Quantification regions: S1 (white dotted rectangle) spans stage 2a and proximal stage 2b of germarium development; S2 (blue outline) demarcates germline based on Vasa staining. The IGS/germline cAMP ratio was calculated as (S1–S2)/S2. All flies were cultured at 29 °C to induce the production of Inx2-CarGAP. (Scale bar, 10 μm.) (*F*) Quantification of relative cAMP levels (IGS/germline) from *E*. Data are presented as mean ± SEM (n = number of germaria); repeated-measures one-way ANOVA with Dunnett's test: ****$P \le 0.0001$; n.s., not significant.

the Inx2-CarGAP system, the production of Inx4-$CarH_C$ in *inx4KD+inx4^{RR}-carH$_C$* proved to be able to rescue the defective development of GSCs and their progeny caused by *inx4KD*, indicative of functional Inx4-CarGAP channels formed by Inx4-$CarH_C$ and Inx2 (Fig. 5 *E–H*). Feeding the *inx4KD+inx4^{RR}-carH$_C$* flies with $AdoB_{12}$, but not MeB_{12}, induced ovarian defects,

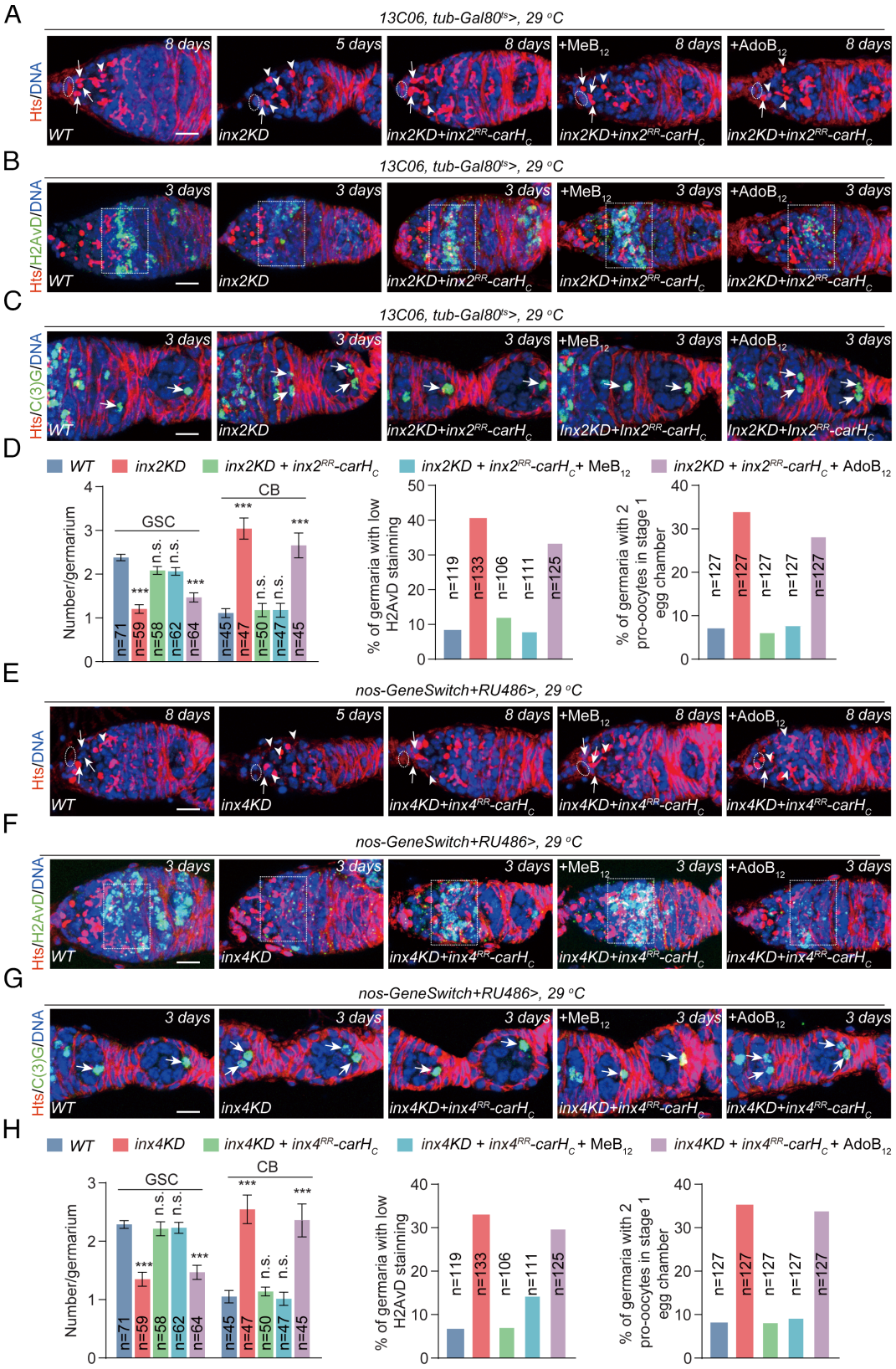

Fig. 5. $AdoB_{12}$-induced gap junction blockage in *Drosophila* germaria. (*A*) Germline stem cell (GSC) and cystoblast (CB) populations under Inx2-CarGAP conditions. Spectrosomes in GSCs/CBs and fusomes in cysts were labeled with the marker Hts. Cap cells (dashed outlines) define the niche; adjacent germ cells are GSCs (arrows). Arrowheads indicate CBs. All cultures at 29 °C. (Scale bar, 10 μm.) (*B*) H2AvD expression marking DNA double-strand breaks in meiotic 16-cell cysts. All cultures at 29 °C. (Scale bar, 10 μm.) (*C*) Stage 1 egg chambers showing oocyte specification (arrows). All cultures at 29 °C. (Scale bar, 10 μm.) (*D*) Quantification of GSC/CB counts (*Left*), H2AvD-positive cysts (middle), and oocyte-containing egg chambers (*Right*). Data are presented as mean ± SEM (n = germaria count); Student's *t* test: ***$P \le 0.001$; n.s., not significant. (*E*) GSC and CB populations under Inx4-CarGAP conditions. Cap cells (dashed outlines), GSCs (arrows), CBs (arrowheads). Cultures at 29 °C. (Scale bar, 10 μm.) (*F*) H2AvD expression in meiotic 16-cell cysts (29 °C). (Scale bar, 10 μm.) (*G*) Oocyte incidence in stage 1 egg chambers (arrows; 29 °C). (Scale bar, 10 μm.) (*H*) Quantification of GSC/CB counts (*Left*), H2AvD-positive cysts (*Middle*), and oocyte formation (*Right*). Data are presented as mean ± SEM (n = germaria count); Student's *t* test: ***$P \le 0.001$; n.s., not significant.

such as GSC loss, CB accumulation, defective meiotic DSB formation and aberrant oocyte determination, comparable to *inx4* knockdown (i.e., *inx4KD*) (Fig. 5 *E–H*). It is noteworthy that the developmental anomalies caused by $AdoB_{12}$-induced CarGAP blockage were somewhat milder than those by gene silencing in *inx2KD* and *inx4KD,* the latter of which exhibited severe aberrations in germarium shape, including drastic reduction in size and loss of contour (Fig. 5 *A* and *E*). The phenotypic differences between chemogenetic inhibition and gene knockout might stem from two possible mechanisms. First, the $AdoB_{12}$-induced gap junction blockage may incompletely suppress metabolite transfer through innexin channels due to their larger pore size compared to connexins. Second, it is very likely that the pleiotropic functions of innexins beyond channel activity, including those in cell tiling (70), cell adhesion (71), and cytoskeletal stabilization (72), still persist even when channel function is chemically inhibited, which may contribute to distinct phenotypic outcomes (73). These results established CarGAP, with oral administration of $AdoB_{12}$, as a convenient molecular tool for controlling gap junctions in vivo.

Discussion and Conclusions

Since the first electron micrograph of gap junctions was obtained over sixty years ago (74), researchers have sought to understand their critical roles in rapid signal transduction and electrical coupling across multicellular structures. However, reliable tools for noninvasive control and interrogation of these intercellular channels remain elusive. While optogenetic approaches offer theoretical precision, practical limitations persist: light delivery challenges in vivo and problematic dark-state activity in common tools like rhodopsins and Cry2 domains that often compromise data accuracy (75). Chemogenetic methods using small molecules can circumvent some delivery issues, but existing standards like rapamycin present their own constraints. Though widely adopted for FKBP-FRB dimerization in vitro (76) and in vivo (77), rapamycin's inhibition of mTOR signaling (78, 79)—which directly impacts the trafficking of gap junction proteins (80)—limits its utility for studying intercellular communication.

CarGAP combines the strengths of both approaches. Built around the compact (~23 kDa; comparable to GFP), B_{12}-dependent photoreceptor $CarH_C$, this system leverages the unique advantages of vitamin B_{12}: marked green-light sensitivity [10 mW/cm^2—at least three orders of magnitude lower than conventional CALI methods (29, 30)], exceptional biocompatibility (81), and the ability to cross the blood–brain barrier when administered orally (82). Unlike signaling-active molecules, vitamin B_{12} has not been known for any pronounced role in biological signaling and mainly serves as a nutrient, particularly crucial for neural function (82). By integrating the precision of optogenetics with the tissue penetration of chemogenetics, CarGAP may finally enable rigorous investigation of GJC-mediated signaling in complex biological systems, including the nervous system.

This study has demonstrated the B_{12}-dependent CarGAP system as a versatile chemo-optogenetic tool for investigating GJC-mediated signaling in mammalian cell cultures and *Drosophila* ovaries. In N2A cells, connexin-based CarGAP enabled precise control of intercellular 2',3'-cGAMP transport and subsequent cGAS-STING activation in neighboring cells, a crucial process in bystander immunity. When combined with the far-red fluorescent voltage indicator NAVI-Cy5, this system permitted rapid, reversible modulation and optical monitoring of electrical coupling in cell clusters. The conserved architecture of gap junction proteins suggests broad applicability of the CarGAP design principle across different biological systems.

We successfully adapted CarGAP to invertebrate gap junctions, creating an innexin-based version that regulates cAMP flow from somatic niche cells to germline in *Drosophila* ovaries. This enabled stepwise control of germ cell development. Unlike genetic approaches that eliminate all protein functions, $AdoB_{12}$-induced $CarH_C$ oligomerization specifically blocks CarGAP's channel activity while preserving nonchannel roles (e.g., structural scaffolding and cell adhesion). This selectivity revealed previously obscured nuances in gap junction function within complex biological systems.

Given the established importance of gap junction-mediated signaling in mammalian development and disease (83, 84), CarGAP represents a powerful and versatile synthetic biology platform. Its vitamin B_{12} dependency provides a simple, unified control axis for interrogating complex developmental processes and disease mechanisms, obviating the need for complex, multicomponent induction schemes. By integrating B_{12}-mediated inhibition with optical reactivation, CarGAP enables programmable synthetic cell–cell communication (85), allows precise patterning and tuning of intercellular coupling in engineered tissues and organs-on-chips to probe emergent tissue-level phenomena (86), and supports optogenetics-based small-molecule screening by optically linking junctional states to functional readouts (87). Together, these capabilities open broad avenues for dissecting intercellular communication across diverse biological contexts and for systematically mapping how junctional connectivity shapes development, physiology, and pathology.

In summary, we have developed CarGAP, a versatile molecular tool that enables reversible control of GJCs across biological systems—from mammalian cell cultures to *Drosophila* ovaries in vivo. This system centers on the chemo-optogenetic switch $CarH_C$, which undergoes $AdoB_{12}$-dependent oligomerization and light-triggered disassembly. By combining vitamin B_{12} administration with green light illumination, CarGAP effectively modulates both chemical signaling (including second messengers like 2',3'-cGAMP and cAMP) and electrical coupling between connected cells. Our application of this tool has revealed fundamental aspects of heterotypic gap junction function during *Drosophila* ovarian development. The generalizable design principle of CarGAP promises to advance our understanding of intercellular communication mechanisms that are fundamental to multicellular life.

Materials and Methods

Gap-junctional communication was assayed by coculturing dye-loaded donor Neuro-2A cells with unlabeled recipients, followed by fluorescence imaging and flow cytometry to quantify transfer. Electrical coupling was controlled and monitored in a Cx43KO + Cx43-$CarH_C$ HeLa line using NAVI-Cy5 in combination with whole-cell patch clamp and concurrent voltage imaging. For in vivo tests, Drosophila were supplemented with vitamin B_{12} on food, maintained in darkness, and processed after defined light exposure. Light regimens were tailored to each assay, and "dark" conditions denote rigorous light shielding during treatment with only brief endpoint imaging. Detailed experimental procedures are available in *SI Appendix*, Experimental Procedures. See *SI Appendix*, Table S1 for the list of DNA sequences used in this study.

Data, Materials, and Software Availability. All study data are included in the article and/or *SI Appendix*.

ACKNOWLEDGMENTS. This work was supported by the Ministry of Science and Technology (2020YFA0908100, F.S.), the Research Fellow Scheme (RFS2324-6S05, F.S.), the Young Collaborative Research Fund (C6001-23Y, F.S.), the Theme-Based Research Scheme (T13-602/21-N, T.X.), the Research Grants Council of Hong Kong SAR (GRF #16103421, F.S.), the Research Institute of Tsinghua, Pearl River Delta (#RITPRD21EG01, F.S.), and the Natural Science Foundation of China Excellent Young Scientists Fund (22122707, F.S.).

Author affiliations: [a]Department of Chemical and Biological Engineering, The Hong Kong University of Science and Technology, Kowloon, Hong Kong SAR, China; [b]College of Chemistry and Molecular Engineering, Synthetic and Functional Biomolecules Center, Beijing National Laboratory for Molecular Sciences, Key Laboratory of Bioorganic Chemistry and Molecular Engineering of the Ministry of Education, Peking University, Beijing 100871, China; [c]Division of Life Science, The Hong Kong University of Science and Technology, Kowloon, Hong Kong SAR, China; [d]School of Life Science and Technology, Southeast University, Nanjing 210031, China; [e]Biomedical Research Institute, Shenzhen Peking University–The Hong Kong University of Science and Technology Medical Center, Shenzhen 518036, China; and [f]Shenzhen Bay Laboratory, Shenzhen 518036, China

1. N. M. Kumar, N. B. Gilula, The gap junction communication channel. *Cell* **84**, 381–388 (1996).
2. I. M. Skerrett, J. B. Williams, A structural and functional comparison of gap junction channels composed of connexins and innexins. *Dev. Neurobiol.* **77**, 522–547 (2017).
3. G. Welzel, S. Schuster, Connexins evolved after early chordates lost innexin diversity. *Elife* **11**, e74422 (2022).
4. V. Verselis, R. White, D. Spray, M. Bennett, Gap junctional conductance and permeability are linearly related. *Science* **234**, 461–464 (1986).
5. R. Tu *et al.*, Gap junction–transported cAMP from the niche controls stem cell progeny differentiation. *Proc. Natl. Acad. Sci.* **120**, e2304168120 (2023).
6. A. Ablasser *et al.*, Cell intrinsic immunity spreads to bystander cells via the intercellular transfer of cGAMP. *Nature* **503**, 530–534 (2013).
7. Q. Chen *et al.*, Carcinoma–astrocyte gap junctions promote brain metastasis by cGAMP transfer. *Nature* **533**, 493–498 (2016).
8. E. Kizana, E. Cingolani, E. Marban, Non-cell-autonomous effects of vector-expressed regulatory RNAs in mammalian heart cells. *Gene Ther.* **16**, 1163–1168 (2009).
9. C. Vachias *et al.*, Gap junctions allow transfer of metabolites between germ cells and somatic cells to promote germ cell growth in the *Drosophila* ovary. *PLoS Biol.* **23**, e3003045 (2025).
10. J. Neijssen *et al.*, Cross-presentation by intercellular peptide transfer through gap junctions. *Nature* **434**, 83–88 (2005).
11. H. J. Jongsma, R. Wilders, Gap junctions in cardiovascular disease. *Circ. Res.* **86**, 1193–1197 (2000).
12. S. A. Bloomfield, B. Völgyi, The diverse functional roles and regulation of neuronal gap junctions in the retina. *Nat. Rev. Neurosci.* **10**, 495–506 (2009).
13. A. Almoril-Porras *et al.*, Configuration of electrical synapses filters sensory information to drive behavioral choices. *Cell* **188**, 89–103.e13 (2024).
14. Y. Zhu, H. Zhu, P. Wu, Gap junctions in polycystic ovary syndrome: Implications for follicular arrest. *Dev. Dyn.* **253**, 882–894 (2024).
15. T. Aasen, M. Mesnil, C. C. Naus, P. D. Lampe, D. W. Laird, Gap junctions and cancer: Communicating for 50 years. *Nat. Rev. Cancer* **16**, 775–788 (2016).
16. D. Spray, J. Stern, A. Harris, M. Bennett, Gap junctional conductance: comparison of sensitivities to H and Ca ions. *Proc. Natl. Acad. Sci.* **79**, 441–445 (1982).
17. C. Peracchia, Chemical gating of gap junction channels: Roles of calcium, pH and calmodulin. *Biochimica et Biophysica Acta (BBA)-Biomembranes* **1662**, 61–80 (2004).
18. J. C. Sáez, V. M. Berthoud, M. C. Branes, A. D. Martínez, E. C. Beyer, Plasma membrane channels formed by connexins: Their regulation and functions. *Physiol. Rev.* **83**, 1359–1400 (2003).
19. S. Caveney, The role of gap junctions in development. *Annu. Rev. Physiol.* **47**, 319–335 (1985).
20. O. Krüger *et al.*, Defective vascular development in connexin 45-deficient mice. *Development* **127**, 4179–4193 (2000).
21. H.-D. Gabriel *et al.*, Transplacental uptake of glucose is decreased in embryonic lethal connexin26-deficient mice. *J. Cell Biol.* **140**, 1453–1461 (1998).
22. A. E. Pereda, Electrical synapses and their functional interactions with chemical synapses. *Nat. Rev. Neurosci.* **15**, 250–263 (2014).
23. B. R. Rost, J. Wietek, O. Yizhar, D. Schmitz, Optogenetics at the presynapse. *Nat. Neurosci.* **25**, 984–998 (2022).
24. A. Y. Karpova, D. G. Tervo, N. W. Gray, K. Svoboda, Rapid and reversible chemical inactivation of synaptic transmission in genetically targeted neurons. *Neuron* **48**, 727–735 (2005).
25. K. Ojima *et al.*, Coordination chemogenetics for activation of GPCR-type glutamate receptors in brain tissue. *Nat. Commun.* **13**, 3167 (2022).
26. R. Rozental, M. Srinivas, D. C. Spray, How to close a gap junction channel: Efficacies and potencies of uncoupling agents. *Methods Mol. Biol.* **154**, 447–476 (2001).
27. G. R. Juszczak, A. H. Swiergiel, Properties of gap junction blockers and their behavioural, cognitive and electrophysiological effects: Animal and human studies. *Prog. Neuropsychopharmacol. Biol. Psychiatry* **33**, 181–198 (2009).
28. T. Desplantez, V. Verma, L. Leybaert, W. Evans, R. Weingart, Gap26, a connexin mimetic peptide, inhibits currents carried by connexin43 hemichannels and gap junction channels. *Pharmacol. Res.* **65**, 546–552 (2012).
29. T. Tanabe *et al.*, Multiphoton excitation–evoked chromophore-assisted laser inactivation using green fluorescent protein. *Nat. Methods* **2**, 503–505 (2005).
30. O. Tour, R. M. Meijer, D. A. Zacharias, S. R. Adams, R. Y. Tsien, Genetically targeted chromophore-assisted light inactivation. *Nat. Biotechnol.* **21**, 1505–1508 (2003).
31. M. E. Bulina *et al.*, A genetically encoded photosensitizer. *Nat. Biotechnol.* **24**, 95–99 (2006).
32. W. Zhang *et al.*, Optogenetic control with a photocleavable protein. PhoCl. *Nat. Methods* **14**, 391–394 (2017).
33. E. S. Boyden, F. Zhang, E. Bamberg, G. Nagel, K. Deisseroth, Millisecond-timescale, genetically targeted optical control of neural activity. *Nat. Neurosci.* **8**, 1263–1268 (2005).
34. K. Kolar, C. Knobloch, H. Stork, M. Žnidarič, W. Weber, Optobase: A web platform for molecular optogenetics. *ACS Synth. Biol.* **7**, 1825–1828 (2018).
35. A.-M. Tichy, E. J. Gerrard, J. M. Legrand, R. M. Hobbs, H. Janovjak, Engineering strategy and vector library for the rapid generation of modular light-controlled protein–protein interactions. *J. Mol. Biol.* **431**, 3046–3055 (2019).
36. R. Wang, Z. Yang, J. Luo, I.-M. Hsing, F. Sun, B12-dependent photoresponsive protein hydrogels for controlled stem cell/protein release. *Proc. Natl. Acad. Sci.* **114**, 5912–5917 (2017).
37. B. Jiang *et al.*, Injectable, photoresponsive hydrogels for delivering neuroprotective proteins enabled by metal-directed protein assembly. *Sci. Adv.* **6**, eabc4824 (2020).
38. S. Kainrath, M. Stadler, E. Reichhart, M. Distel, H. Janovjak, Green-light-induced inactivation of receptor signaling using cobalamin-binding domains. *Angew. Chem. Int. Ed.* **56**, 4608–4611 (2017).
39. M. Mansouri *et al.*, Smart-watch-programmed green-light-operated percutaneous control of therapeutic transgenes. *Nat. Commun.* **12**, 3388 (2021).
40. R. J. Kutta *et al.*, The photochemical mechanism of a B12-dependent photoreceptor protein. *Nat. Commun.* **6**, 7907 (2015).
41. M. Jost *et al.*, Structural basis for gene regulation by a B12-dependent photoreceptor. *Nature* **526**, 536–541 (2015).
42. S. Padmanabhan, M. Jost, C. L. Drennan, M. Elías-Arnanz, A new facet of vitamin B12: Gene regulation by cobalamin-based photoreceptors. *Annu. Rev. Biochem.* **86**, 485–514 (2017).
43. C. Chatelle *et al.*, A green-light-responsive system for the control of transgene expression in mammalian and plant cells. *ACS Synth. Biol.* **7**, 1349–1358 (2018).
44. M. Yeager, B. J. Nicholson, Structure of gap junction intercellular channels. *Curr. Opin. Struct. Biol.* **6**, 183–192 (1996).
45. E. C. Beyer, D. L. Paul, D. A. Goodenough, Connexin43: A protein from rat heart homologous to a gap junction protein from liver. *J. Cell Biol.* **105**, 2621–2629 (1987).
46. K. Jordan *et al.*, Trafficking, assembly, and function of a connexin43-green fluorescent protein chimera in live mammalian cells. *Mol. Biol. Cell* **10**, 2033–2050 (1999).
47. R. E. Campbell *et al.*, A monomeric red fluorescent protein. *Proc. Natl. Acad. Sci.* **99**, 7877–7882 (2002).
48. K. Reed *et al.*, Molecular cloning and functional expression of human connexin37, an endothelial cell gap junction protein. *J. Clin. Invest.* **91**, 997–1004 (1993).
49. H. Chen, Y. X. Li, R. S. Wong, J. L. Esseltine, D. Bai, Genetically engineered human embryonic kidney cells as a novel vehicle for dual patch clamp study of human gap junction channels. *Biochem. J.* **481**, 741–758 (2024).
50. A. Jassim, H. Aoyama, G. Y. Willy, H. Chen, D. Bai, Engineered Cx40 variants increased docking and function of heterotypic Cx40/Cx43 gap junction channels. *J. Mol. Cell. Cardiol.* **90**, 11–20 (2016).
51. G. Y. Willy *et al.*, Junctional delay, frequency, and direction-dependent uncoupling of human heterotypic Cx45/Cx43 gap junction channels. *J. Mol. Cell. Cardiol.* **111**, 17–26 (2017).
52. J. Czyż, U. Irmer, G. Schulz, A. Mindermann, D. F. Hülser, Gap-junctional coupling measured by flow cytometry. *Exp. Cell Res.* **255**, 40–46 (2000).
53. M. H. Juul, E. Rivedal, T. Stokke, T. Sanner, Quantitative determination of gap junction intercellular communication using flow cytometric measurement of fluorescent dye transfer. *Cell Adh. Commun.* **7**, 501–512 (2000).
54. M. J. Nielsen, M. R. Rasmussen, C. B. Andersen, E. Nexø, S. K. Moestrup, Vitamin B12 transport from food to the body's cells–a sophisticated, multistep pathway. *Nat. Rev. Gastroenterol. Hepatol.* **9**, 345–354 (2012).
55. G. G. Gick *et al.*, Cellular uptake of vitamin B12: Role and fate of TCblR/CD320, the transcobalamin receptor. *Exp. Cell Res.* **396**, 112256 (2020).
56. J. R. de Groot *et al.*, Conduction slowing by the gap junctional uncoupler carbenoxolone. *Cardiovasc. Res.* **60**, 288–297 (2003).
57. Z. Yang *et al.*, B12-induced reassembly of split photoreceptor protein enables photoresponsive hydrogels with tunable mechanics. *Sci. Adv.* **8**, eabm5482 (2022).
58. J. Wu, Z. J. Chen, Innate immune sensing and signaling of cytosolic nucleic acids. *Annu. Rev. Immunol.* **32**, 461–488 (2014).
59. S. L. Ergun, D. Fernandez, T. M. Weiss, L. Li, Sting polymer structure reveals mechanisms for activation, hyperactivation, and inhibition. *Cell* **178**, 290–301.e210 (2019).
60. X. Wei *et al.*, LL-37 transports immunoreactive cGAMP to activate STING signaling and enhance interferon-mediated host antiviral immunity. *Cell Rep.* **39**, 110880 (2022).
61. Y. Xu *et al.*, Hybrid indicators for fast and sensitive voltage imaging. *Angew. Chem.* **130**, 4013–4017 (2018).
62. P. Zou *et al.*, Bright and fast multicoloured voltage reporters via electrochromic FRET. *Nat. Commun.* **5**, 4625 (2014).
63. E. J. Choi, N. Palacios-Prado, J. C. Sáez, J. Lee, Identification of Cx45 as a major component of GJs in HeLa cells. *Biomolecules* **10**, 1–14 (2020).
64. P. Phelan, Innexins: Members of an evolutionarily conserved family of gap-junction proteins. *Biochimica et Biophysica Acta (BBA)-Biomembranes* **1711**, 225–245 (2005).
65. D. Kirilly, S. Wang, T. Xie, Self-maintained escort cells form a germline stem cell differentiation niche. *Development* **138**, 5087–5097 (2011).
66. C. H. Zhu, T. Xie, Clonal expansion of ovarian germline stem cells during niche formation in Drosophila. *Development* **130**, 2579–2588 (2003).
67. P. Sahai-Hernandez, T. G. Nystul, A dynamic population of stromal cells contributes to the follicle stem cell niche in the *Drosophila* ovary. *Development* **140**, 4490–4498 (2013).
68. M. Van Doren, A. L. Williamson, R. Lehmann, Regulation of zygotic gene expression in *Drosophila* primordial germ cells. *Curr. Biol.* **8**, 243–246 (1998).
69. T. Osterwalder, K. S. Yoon, B. H. White, H. Keshishian, A conditional tissue-specific transgene expression system using inducible GAL4. *Proc. Natl. Acad. Sci.* **98**, 12596–12601 (2001).
70. A. Hendi *et al.*, Channel-independent function of UNC-9/Innexin in spatial arrangement of GABAergic synapses in *C. elegans*. *Elife* **11**, e80555 (2022).
71. M. Das, D. Cheng, T. Matzat, V. J. Auld, Innexin-mediated adhesion between glia is required for axon ensheathment in the peripheral nervous system. *J. Neurosci.* **43**, 2260–2276 (2023).
72. G. Miao, D. Godt, D. J. Montell, Integration of migratory cells into a new site in vivo requires channel-independent functions of innexins on microtubules. *Dev. Cell* **54**, 501–515.e509 (2020).
73. D. A. Goodenough, D. L. Paul, Beyond the gap: Functions of unpaired connexon channels. *Nat. Rev. Mol. Cell Biol.* **4**, 285–295 (2003).
74. F. Sjöstrand, E. Andersson-Cedergren, M. Dewey, The ultrastructure of the intercalated discs of frog, mouse and guinea pig cardiac muscle. *J. Ultrastruct. Res.* **1**, 271–287 (1958).
75. T. Kyung *et al.*, Optogenetic control of endogenous Ca2+ channels *in vivo*. *Nat. Biotechnol.* **33**, 1092–1096 (2015).
76. L. A. Banaszynski, C. W. Liu, T. J. Wandless, Characterization of the FKBP⊙ rapamycin⊙ FRB ternary complex. *J. Am. Chem. Soc.* **127**, 4715–4721 (2005).
77. Q. Zhang *et al.*, Visualizing dynamics of cell signaling in vivo with a phase separation-based kinase reporter. *Mol. Cell* **69**, 334–346.e334 (2018).
78. J. Li, S. G. Kim, J. Blenis, Rapamycin: One drug, many effects. *Cell Metab.* **19**, 373–379 (2014).
79. M. Laplante, D. M., mTOR signaling in growth control and disease. *Cell* **149**, 274–293 (2012).
80. J. W. Smyth, R. M. Shaw, Autoregulation of connexin43 gap junction formation by internally translated isoforms. *Cell Rep.* **5**, 611–618 (2013).

81. Institute of Medicine (US) Standing Committee on the Scientific Evaluation of Dietary Reference Intakes and its Panel on Folate, Other B Vitamins, and Choline, Dietary reference intakes for thiamin, riboflavin, niacin, vitamin B6, folate, vitamin B12, pantothenic acid, biotin, and choline (2000).
82. W. Roth, M. Mohamadzadeh, Vitamin B12 and gut-brain homeostasis in the pathophysiology of ischemic stroke. *EBioMedicine* **73**, 103676 (2021).
83. C. J. Wei, X. Xu, C. W. Lo, Connexins and cell signaling in development and disease. *Annu. Rev. Cell Dev. Biol.* **20**, 811–838 (2004).
84. D. A. Goodenough, D. L. Paul, Gap junctions. *Cold Spring Harb. Perspect. Biol.* **1**, a002576 (2009).
85. R. Chait, J. Ruess, T. Bergmiller, G. Tkačik, C. C. Guet, Shaping bacterial population behavior through computer-interfaced control of individual cells. *Nat. Commun.* **8**, 1535 (2017).
86. D. Mao, N. Li, Z. Xiong, Y. Sun, G. Xu, Single-cell optogenetic control of calcium signaling with a high-density micro-LED array. *Iscience* **21**, 403–412 (2019).
87. V. Agus, H. Janovjak, Optogenetic methods in drug screening: Technologies and applications. *Curr. Opin. Biotechnol.* **48**, 8–14 (2017).